Evolving Technology

Electromechanical characterization of a tissue-engineered myocardial patch derived from extracellular matrix

Takeyoshi Ota, MD, PhD,[a] Thomas W. Gilbert, PhD,[b] Stephen F. Badylak, DVM, MD, PhD,[b] David Schwartzman, MD,[c] and Marco A. Zenati, MD[a]

Objective: Extracellular matrix scaffolds have been successfully used for myocardial wall repair. However, regional functional evaluation (ie, contractility, electrical conductivity) of the extracellular matrix scaffold during the course of remodeling has been limited. In the present study, we evaluated the remodeled scaffold for evidence of electrical activation.

Methods: The extracellular matrix patch was implanted into the porcine right ventricular wall (n = 5) to repair an experimentally produced defect. Electromechanical mapping was performed with the NOGA system (Biosense Webster Inc, Diamond Bar, Calif) 60 days after implantation. Linear local shortening was recorded to assess regional contractility. After sacrifice, detailed histologic examinations were performed.

Results: Histologic examinations showed repopulation of the scaffold with cells, including a monolayer of factor VIII–positive cells in the endocardial surface and multilayered α-smooth muscle actin–positive cells beneath the monolayer cells. The α-smooth muscle actin–positive cells tended to be present at the endocardial aspect of the remodeled scaffold and at the border between the remodeled scaffold and the normal myocardium. Electromechanical mapping demonstrated that the patch had low-level electrical activity (0.56 ± 0.37 mV; $P < .0001$) in most areas and moderate activity (2.20 ± 0.70 mV; $P < .0001$) in the margin between the patch and the normal myocardium (7.58 ± 2.23 mV).

Conclusions: The extracellular matrix scaffolds were repopulated by α-smooth muscle actin–positive cells 60 days after implantation into the porcine heart. The presence of the cells corresponded to areas of the remodeling scaffold that showed early signs of electrical conductivity.

ET

Heart failure is a major health problem with increasing prevalence, caused in part by the increased survivals for patients who have had acute myocardial infarction, increased life expectancy, and lifestyle choices. Postinfarction left ventricular (LV) remodeling is characterized by LV dilatation and abnormal geometry including development of LV aneurysm leading to congestive heart failure.

Although heart transplantation is currently the best surgical option for this disease, there are many practical reasons for not making it the first choice for every patient. A shortage of donor organs and increased age, pulmonary hypertension, and

Abbreviations and Acronyms
ECM = extracellular matrix
ICE = intracardiac echocardiography
LLS = linear local shortening
LV = left ventricular
LVAS = left ventricular assist system(s)
RV = right ventricular
SMA = smooth muscle actin
SVR = surgical ventricular restoration
UBM = urinary bladder matrix

chronic organ failure of the recipient are factors that limit the number of heart transplants, which reached a plateau in recent years.[1] There are about 50,000 deaths per year related to congestive heart failure, yet there are only about 2000 heart transplantations per year.[2] Mechanical support technologies such as LV assist systems (LVAS) have been developed to compensate for the lack of available donor organs and as a bridge to transplantation. However, this therapy is limited by infection, cost, durability, and thromboembolism.[3]

Surgical ventricular restoration (SVR) is an important strategy for effective treatment of postinfarction heart failure. Most SVR, like the septal anterior ventricular exclusion or the Calafiore procedures, involves the placement of a synthetic cardiac patch, such as Dacron and Teflon, to restore the geometry of the heart.[4,5] These patches are inert materials that are rapidly encapsulated by the host and do not restore myocardial function. For SVR to serve as a replacement for transplantation as opposed to a temporary delay, new patch materials that promote the formation of functional myocardial tissue will be required.

Recently, naturally occurring extracellular matrix (ECM) scaffolds have been successfully used for the repair of a variety of tissues in preclinical studies and clinical applications.[6-9] ECM is degraded quickly after implantation and promotes site-specific tissue remodeling. Urinary bladder matrix (UBM) is one such promising ECM scaffold material that has shown promise for myocardial repair.[10-13] Kochupura and associates[12] demonstrated that a UBM scaffold placed in right ventricular (RV) walls of dogs was repopulated by myocytes. The remodeled UBM scaffold restored some regional mechanical function as determined with computer-aided speckle interferometry. Robinson and colleagues[13] showed successful replacement of LV wall defects in a porcine model using UBM scaffolds, but regional function was not evaluated.

The current study was designed to confirm the finding that an ECM scaffold used to repair the myocardial wall is repopulated by myocytes in a porcine model. Inasmuch as it was shown previously that a UBM patch improves the global and regional function of the heart, the current study

also aimed to determine whether the myocytes contributed electromechanical function to the remodeled UBM scaffold. Electromechanical assessment was performed with a NOGA-Star mapping system (Biosense Webster Inc, Diamond Bar, Calif) with an intracardiac echocardiography (ICE) system. There is typically a direct relationship between electrophysiologic parameter with NOGA and myocardial viability.[14,15] The combination of the ICE system with the NOGA-Star system permitted stable endocardial contact at each mapped site. In addition, ICE guidance displayed echocardiographically distinct anatomic landmarks (eg, mitral valve leaflets, chordae tendineae, ventricular wall thinning/akinesis/dyskinesis, endocardial thrombus) to aid navigation.

Materials and Methods
UBM Scaffold Preparation
Porcine urinary bladders were harvested from market weight pigs (approximately 110-130 kg) immediately after they were put to death. After repeated washes with tap water, the urothelial layer was removed by soaking of the material in 1N saline. The tunica serosa, tunica muscularis externa, tunica submucosa, and most of the muscularis mucosa were mechanically delaminated from the remaining bladder tissue. The remaining basement membrane of the tunica mucosa and the subjacent tunica propria, collectively termed UBM, were then decellularized and disinfected by immersion in 0.1% peracetic acid and 4% ethanol solution for 2 hours and rinsed in phosphate-buffered saline.[16]

A four-layer construct of the hydrated sheets of UBM was created such that the basement membrane was exposed on either side of the sheet. The four-layer construct was then laminated by a vacuum-pressing technique. The construct was placed between two perforated stainless steel sheets, and the stainless steel plates were placed between sheets of sterile gauze. The entire construct was then sealed in vacuum bagging and subjected to a vacuum of 710 to 730 mm Hg for approximately 8 hours. The final device was 0.1 mm in thickness and terminally sterilized by exposure to ethylene oxide. The device was rehydrated in saline just before the operation.[16] These scaffolds were identical to scaffolds used in a previous study for LV wall repair.[13]

Animal Operations
Five Duroc cross pigs weighing 44 to 50 kg were used. The study was approved by the Institutional Animal Care and Use Committee of the University of Pittsburgh and carried out in compliance with the "Principles of Laboratory Animal Care" formulated by the National Society for Medical Research and the "Guide for the Care and Use of Laboratory Animals" prepared by the National Academy of Sciences and published by the National Institutes of Health (NIH Publication No. 85-23, revised 1985).

Surgical Procedure
Anesthesia was induced with ketamine (20 mg/kg) and xylazine (2 mg/kg) and maintained with 2.0% isoflurane inhalation. The pericardium was opened through a right anterolateral thoracotomy in the fourth intercostal space. After the positioning of a
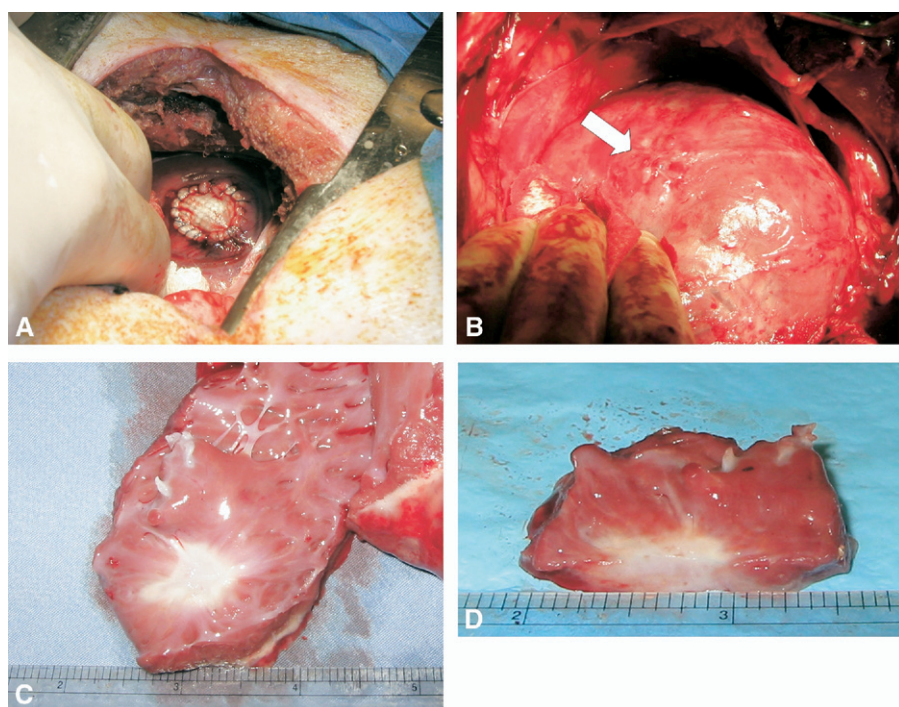
ET

Figure 1. A, Intraoperative view. The tissue-engineered patch is placed on the right ventricular wall. B, No infection and aneurysm are noted on the patch 60 days after implantation *(arrow).* C, Endocardial side of the patch. White tissue is observed. There is no thrombus in the right ventricle. D, Cross section of the patch. The patch region is as thick as the adjoining right ventricular wall.

tangential clamp, a small portion of the RV free wall was substituted with a UBM patch (20 × 20 mm) with a 5-0 continuous polypropylene suture (Figure 1, *A*). The chest was closed. At 60 days after implantation, electrophysiologic mapping was performed, after which the animals were put to death for histologic examination.

Electromechanical Mapping

Electromechanical mapping was performed with the NOGA mapping system. The system uses synchronous extracorporeal magnetic fields projected into the thoracic space to determine the location and orientation of a sensor mounted near the distal electrode of a deflectable bipolar mapping catheter (NOGA-Star, Biosense Webster Inc; 2-mm length tip electrode, 2-mm length ring electrode, 1-mm length interelectrode spacing), which can be used to access the endocardial surface.[17] An ICE system (AcuNAV; Acuson Siemens, Mountain View, Calif) was used together with NOGA to ensure proper placement of the NOGA-Star catheter. The AcuNAV system consists of a 10F deflectable catheter incorporating a phased-array transducer with programmable operating frequency.[18]

Use of NOGA with ICE has been previously described.[19] In brief, the NOGA-Star catheter is introduced into the RV cavity via the right femoral vein. The ICE catheter is placed into the right atrium through the same approach. Endocardial mapping of the entire endocardial surface was performed during sinus rhythm. The acquired point density for non-free RV walls was 5/cm^2; the density for the RV free wall was 10/cm^2.

Mechanical Mapping

Regional contractility was evaluated by calculating the linear local shortening (LLS). The algorithm calculated the fractional shorten-

ing of regional endocardial surface at end-systolic phase as previously described.[20]

Histology and Immunochemistry

Excised tissues were fixed in 10% formalin, embedded in paraffin, cut into 5-μm sections, and placed on a histology slide. The sections were then deparaffinized and either stained with hematoxylin-eosin and Masson trichrome or prepared for immunohistochemical staining. Monoclonal antibodies specific for factor VIII–related antigen (Dako, Carpinteria, Calif) and α-smooth muscle actin (α-SMA) (Dako) were used. The immunoreaction was detected with 3,3-diaminobenzidine.

Statistical Analysis

All values are expressed as the mean $\pm$ standard deviation. The statistical differences in all data were determined by a Mann–Whitney test.

Results

Mortality and Morbidity

All pigs (n = 5) survived without any complications until electively being put to death. The pigs were killed after a mapping 60 days after implantation.

Macroscopic Examination

Neither aneurysm nor infection was noted in the implanted segments at death (Figure 1, *B*). The area of the patch did not change considerably over the course of remodeling. Contraction of the RV wall was uniform, and the patch region was not dyskinetic. The epicardial side of the remod-
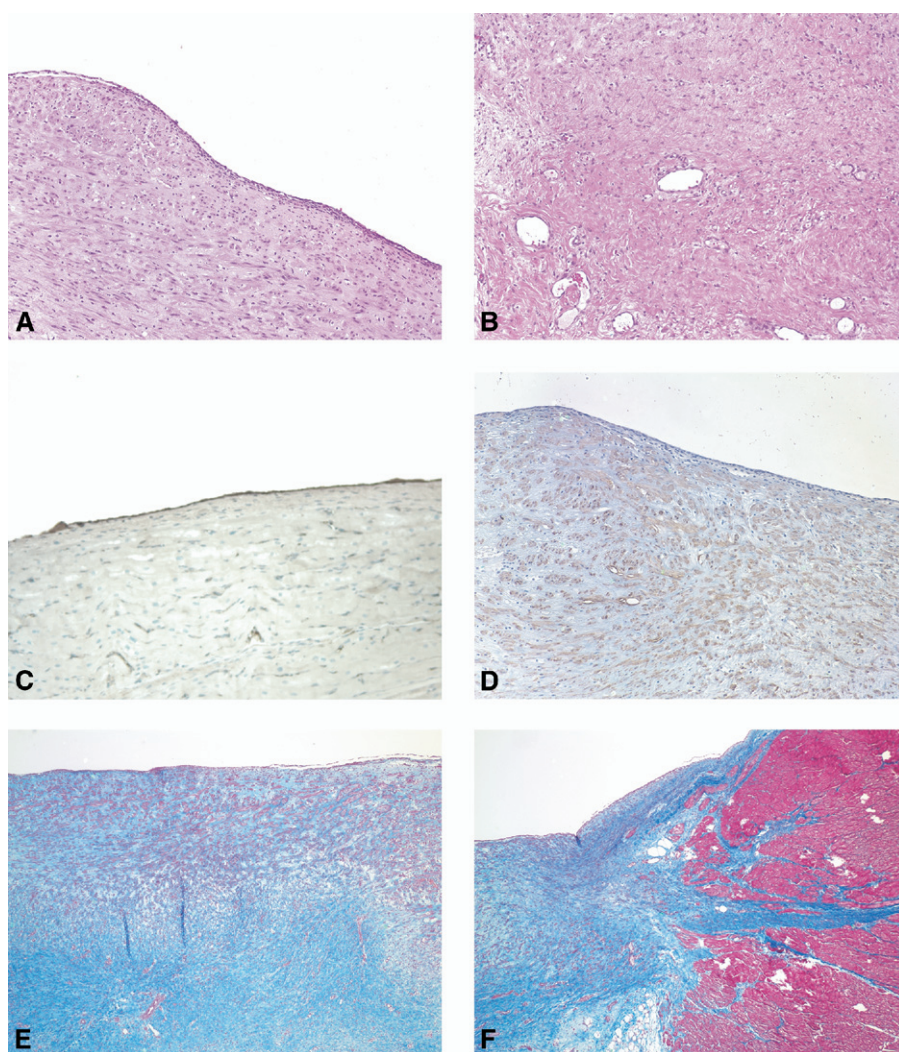
ET

Figure 2. Histologic preparations of the patch 60 days after implantation. A, A good repopulation of cells was observed. B, There was some vasculogenesis in the middle of the patch. C, A monolayer of endothelial cells covered the surface of the tissue. D, Multilayered myocytes were observed beneath the monolayer cells. E, Central part of the patch. Regenerated cells were prone to be unevenly distributed in the endocardial aspect at the around center of the patch. F, Marginal part of the patch. The myocytes extended across full thickness at the edge of the patch. (A and B, hematoxylin–eosin stain; C, factor VIII stain; D, α-smooth muscle actin stain; E and F, Masson trichrome stain. (Magnifications A, B, C, and D ×100; E and F ×40.)

eled UBM scaffold was covered with fibrous connective tissues. The endocardial side of the remodeled tissue was smooth and white with no thrombus around the patch region (Figure 1, C). In a cross section, the whole patch region consisted of white firm tissue. The thickness of the ECM patch increased so that it approached the thickness of the adjacent normal myocardial wall (Figure 1, D).

Histology and Immunochemistry
Sixty days after implantation, the histologic examination of the remodeled UBM scaffold showed a population of round and spindle-shaped cells (Figure 2, A). No evidence for inflammation was noted. Vascularity was noted in the middle and in the epicardial aspect in the remodeled specimen (Figure 2, B). The cells present within the remodeled UBM scaffold consisted of a monolayer of factor VIII–positive cells on the endocardial surface (Figure 2, C) and multilayered α-SMA–positive cells (Figure 2, D) distributed

throughout the remodeled tissue. The Masson trichrome stain showed that the remodeled UBM patch consisted of densely organized collagenous tissue. These cells were present predominantly at the endocardial aspect of the remodeled scaffold and at the margin between the remodeled scaffold and the normal myocardium (Figure 2, E and F).

Electromechanical Mapping
Local unipolar and bipolar voltage electrograms were recorded. More than 200 discrete points were used to map the region of ECM remodeling. The electrical information was presented as 3-dimensional maps displayed in a color-coded fashion (Figure 3). Electrogram amplitude values were graphed out in Figure 4, A. The mean electrogram of the normal myocardial area (displayed in *violet*) was 7.58 ± 2.23 mV. The central part of the patch (displayed in *red*) was representative of abnormal electromechanical function, with low electrical activity (0.56 ± 0.37 mV; $P <$ .0001 vs
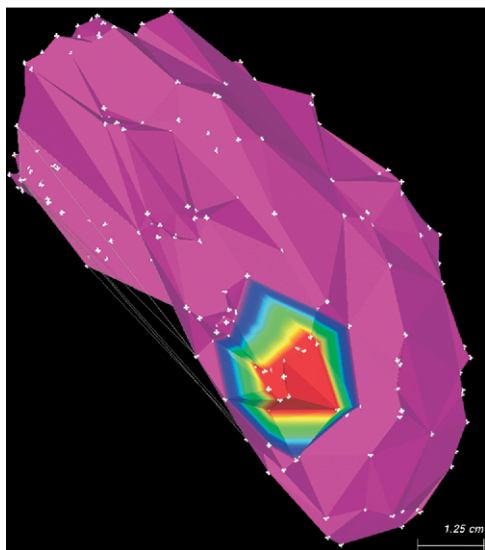
Figure 3. Color-coded electrical map using NOGA. Bipolar electrogram amplitude map. *Red* demarcates peak-to-peak amplitude < 0.5 mV; *violet* > 5.0 mV.

the electrical map in which the mean of electrical amplitude was significantly higher than in the area displayed in *red*.

Discussion

Congestive heart failure is frequently a progressive disease that can be difficult to control with conservative treatment.[21] The final treatment option for patients with end-stage congestive heart failure is transplantation. Inasmuch as there is a shortage of donor organs, SVR has become an important surgical treatment option with demonstrated benefit.[22] However, a limitation of traditional SVR is the use of an inert patch material such as Dacron that cannot remodel into functional myocardial tissue and, as a result, provides no functional improvement to the treated heart. The UBM cardiac patch that has a potential to be functional myocardium can contribute to improving the outcome of SVR.

Recently, a number of tissue-engineered scaffolds have been evaluated for use in myocardial repair, including ECM scaffolds derived from the porcine urinary bladder, as an alternative to synthetic cardiac patches in both the RV and LV wall.[9,11-13,23,24] It has been shown that UBM scaffolds can endure the high-pressure environment of the LV and are rapidly repopulated by a variety of cell types, including cardiac myocytes.[9,11-13] The source of these cells is still under investigation, but recent studies have shown that ECM scaffolds recruit a population of circulating bone marrow–derived cells that may differentiate down a tissue-specific lineage in response to local environmental cues.[25-27] As a result of the this site-specific remodeling, regional mechanical function was improved.[11,12] The results of the current study compare very well with the histologic and mechanical results shown in the previous studies. Histologic examination showed a number of myocytes distributed throughout the remodeled scaffold, with the majority of the cells located at the endocardial aspect and at the junction
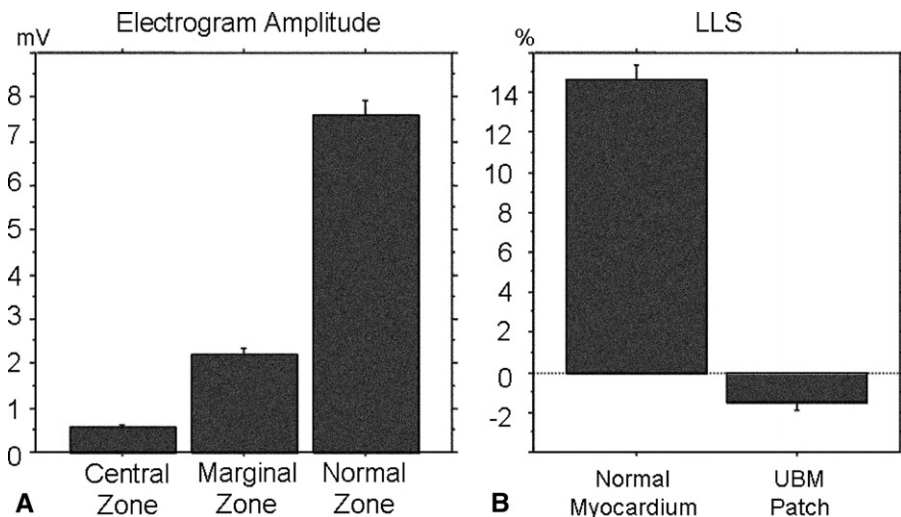
green, violet zone). In the margin between the patch and the normal myocardium, there was a band of moderate electrical activity approximately 5 mm in width (displayed in *green* and *yellow*) that had a mean voltage of 2.20 ± 0.70 mV ($P < .0001$ vs *violet* zone). The LLS was 14.69% ± 4.73% in the normal myocardium and −1.48% ± 2.43% in the UBM patch (Figure 4, *B*). Figure 5 shows a comparison between the patch region of the macrograph and that of the electrical map. Each figure was adjusted in its direction and scale for precise comparison. It demonstrates that the patch region involved the area displayed in *yellow* and *green* in

A

B

Figure 4. A, Electrogram amplitude graph. Central zone corresponds to the area displayed in *red* in Figure 3. Marginal zone corresponds to *yellow* and *green*. Normal zone corresponds to *violet*. B, A graph of the linear local shortening. *LLS,* Linear local shortening; *UBM,* urinary bladder matrix.
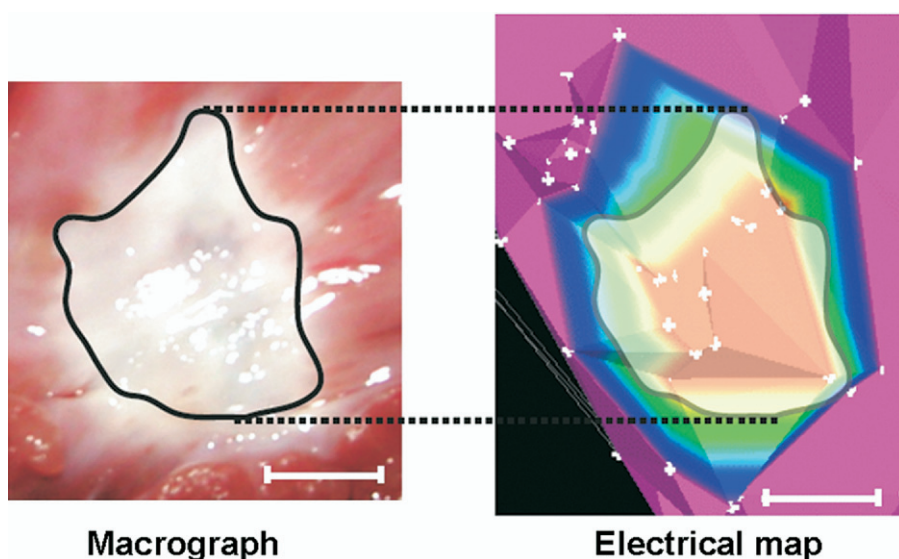
Figure 5. Overlapped figure standardized the scale (*white bar* = 1.25 cm). The patch region includes the marginal zone displayed in *yellow* and *green*.

with the adjacent normal myocardium. Keck and colleagues[14] reported that an LLS threshold of 4% identified significant regional contractility disturbances of akinetic or dyskinetic segments with a specificity of 85% and that of 9% defined a normally contracting segment with a sensitivity of 90%. With a mean LLS below 4%, these results nearly coincided with those of Kochupura and colleagues,[12] suggesting that the regional function of the remodeled scaffold is still immature at 60 days of remodeling. In addition, it demonstrated that regeneration of the electrical activity was not relative to that of the contractility.

These results correspond well with the electrophysiologic function of the remodeled scaffold determined in this study. Although there was essentially no electrical potential in the center of the remodeled scaffold, there was a region of low activity area around the periphery of the remodeling area. The region that showed the greatest electrical potential was co-localized with the region that contained the largest number of cardiac myocytes. It is possible that as remodeling of the ECM scaffold progresses, as suggested by earlier studies,[10] more myocytes would populate the center region of the remodeled graft, further improving the electromechanical properties of the tissue.

Limitations of the present study include evaluation of the electromechanical properties of the remodeling tissue at only one time point and the lack of control experiments in which synthetic cardiac patches were used, inasmuch as this is a preliminary study. Furthermore, the number of animals was relatively small. This study was meant to confirm the findings of previous studies to develop a better understanding of the remodeling of an ECM scaffold in the myocardial location. Longer term studies are planned to determine whether the remodeling of a UBM scaffold progresses and continues to improve the regional cardiac function. Once the

remodeling of an ECM scaffold is fully characterized in a normal heart, future studies will be conducted in a disease-appropriate model (ie, postinfarction heart failure) to determine whether an ECM scaffold remains beneficial.

In conclusion, this study confirms that UBM is a promising scaffold for tissue-engineered cardiac patch repair with no adverse events and that site-appropriate contractile cells participate in the remodeling process. The combination of the NOGA-Star system with the ICE system showed efficacy for evaluating the electromechanical properties of a remodeled tissue-engineered scaffold for cardiac repair.

References

1. Taylor DO, Edwards LB, Boucek MM, Trulock EP, Deng MC, Keck BM, et al. Registry of the International Society for Heart and Lung Transplantation: twenty-second official adult heart transplant report—2005. *J Heart Lung Transplant.* 2005;24:945-55.
2. American Heart Association. Heart and stroke statistical update. Dallas [TX]: American Heart Association; 2002.
3. El-Banayosy A, Korfer R, Arusoglu L, Kizner L, Morshuis M, Milting H, et al. Device and patient management in a bridge-to-transplant setting. *Ann Thorac Surg.* 2001;71:S98-102; discussion S114-5.
4. Calafiore AM, Mauro MD, Di Giammarco G, Gallina S, Iaco AL, Contini M, et al. Septal reshaping for exclusion of anteroseptal dyskinetic or akinetic areas. *Ann Thorac Surg.* 2004;77:2115-21.
5. Suma H, Isomura T, Horii T, Nomura F. Septal anterior ventricular exclusion procedure for idiopathic dilated cardiomyopathy. *Ann Thorac Surg.* 2006;82:1344-8.
6. Badylak S, Kokini K, Tullius B, Whitson B. Strength over time of a resorbable bioscaffold for body wall repair in a dog model. *J Surg Res.* 2001;99:282-7.
7. Badylak SF. Xenogeneic extracellular matrix as a scaffold for tissue reconstruction. *Transplant Immunol.* 2004;12:367-77.
8. Badylak SF, Tullius R, Kokini K, Shelbourne KD, Klootwyk T, Voytik SL, et al. The use of xenogeneic small intestinal submucosa as a biomaterial for Achilles tendon repair in a dog model. *J Biomed Mater Res.* 1995;29:977-85.
9. Badylak SF, Vorp DA, Spievack AR, Simmons-Byrd A, Hanke J, Freytes DO, et al. Esophageal reconstruction with ECM and muscle tissue in a dog model. *J Surg Res.* 2005;128:87-97.

10. Badylak S, Obermiller J, Geddes L, Matheny R. Extracellular matrix for myocardial repair. *Heart Surg Forum.* 2003;6:E20-6.

11. Badylak SF, Kochupura PV, Cohen IS, Doronin SV, Saltman AE, Gilbert TW, et al. The use of extracellular matrix as an inductive scaffold for the partial replacement of functional myocardium. *Cell Transplant.* 2006;15:29-40.

12. Kochupura PV, Azeloglu EU, Kelly DJ, Doronin SV, Badylak SF, Krukenkamp IB, et al. Tissue-engineered myocardial patch derived from extracellular matrix provides regional mechanical function. *Circulation.* 2005;112:I144-9.

13. Robinson KA, Li J, Mathison M, Redkar A, Cui J, Chronos NA, et al. Extracellular matrix scaffold for cardiac repair. *Circulation.* 2005; 112(suppl):I135-43.

14. Keck A, Hertting K, Schwartz Y, Kitzing R, Weber M, Leisner B, et al. Electromechanical mapping for determination of myocardial contractility and viability. A comparison with echocardiography, myocardial single-photon emission computed tomography, and positron emission tomography. *J Am Coll Cardiol.* 2002;40:1067-74; discussion 1075-8.

15. Kornowski R, Hong MK, Leon MB. Comparison between left ventricular electromechanical mapping and radionuclide perfusion imaging for detection of myocardial viability. *Circulation.* 1998;98:1837-41.

16. Freytes DO, Badylak SF, Webster TJ, Geddes LA, Rundell AE. Biaxial strength of multilaminated extracellular matrix scaffolds. *Biomaterials.* 2004;25:2353-61.

17. Gepstein L, Hayam G, Shpun S, Ben-Haim SA. Hemodynamic evaluation of the heart with a nonfluoroscopic electromechanical mapping technique. *Circulation.* 1997;96:3672-80.

18. Packer DL, Stevens CL, Curley MG, Bruce CJ, Miller FA, Khandheria BK, et al. Intracardiac phased-array imaging: methods and initial clinical experience with high resolution, under blood visualization: initial experience with intracardiac phased-array ultrasound. *J Am Coll Cardiol.* 2002;39:509-16.

19. Schwartzman D, Bonanomi G, Zenati MA. Epicardium-based left atrial ablation: impact on electromechanical properties. *J Cardiovasc Electrophysiol.* 2003;14:1087-92.

20. Gepstein L, Goldin A, Lessick J, Hayam G, Shpun S, Schwartz Y, et al. Electromechanical characterization of chronic myocardial infarction in the canine coronary occlusion model. *Circulation.* 1998;98: 2055-64.

21. Jessup M, Brozena S. Heart failure. *N Engl J Med.* 2003;348:2007-18.

22. Athanasuleas CL, Buckberg GD, Stanley AW, Siler W, Dor V, Di Donato M, et al. Surgical ventricular restoration: the RESTORE Group experience. *Heart Fail Rev.* 2004;9:287-97.

23. Chang Y, Chen SC, Wei HJ, Wu TJ, Liang HC, Lai PH, et al. Tissue regeneration observed in a porous acellular bovine pericardium used to repair a myocardial defect in the right ventricle of a rat model. *J Thorac Cardiovasc Surg.* 2005;130:705-11.

24. Iwai S, Sawa Y, Taketani S, Torikai K, Hirakawa K, Matsuda H. Novel tissue-engineered biodegradable material for reconstruction of vascular wall. *Ann Thorac Surg.* 2005;80:1821-7.

25. Badylak SF, Park K, Peppas N, McCabe G, Yoder M. Marrow-derived cells populate scaffolds composed of xenogeneic extracellular matrix. *Exp Hematol.* 2001;29:1310-8.

26. Brountzos E, Pavcnik D, Timmermans HA, Corless C, Uchida BT, Nihsen ES, et al. Remodeling of suspended small intestinal submucosa venous valve: an experimental study in sheep to assess the host cells' origin. *J Vasc Interv Radiol.* 2003;14:349-56.

27. Zantop T, Gilbert TW, Yoder M, Badylak SF. Extracellular matrix scaffolds are repopulated by bone marrow–derived cells in a mouse model of Achilles tendon reconstruction. *J Orthop Res.* 2006;24:1299-309.

ET

Online—www.aats.org

Now you can get *The Journal of Thoracic and Cardiovascular Surgery* online. The Journal online brings you faster delivery time, easy searching of current and back issues, links to PubMed, AATS, WTSA, and other important sites, and more. Visit the Journal online today.

Receive tables of contents by e-mail

To receive the tables of contents by e-mail, sign up through our Web site at *http://journals.elsevierhealth.com/periodicals/ymtc*

Choose *E-mail Notification*

Simply type your e-mail address in the box and click the *Subscribe* button.

You will receive an e-mail to confirm that you have been added to the mailing list.

Note that TOC e-mails will be sent out when a new issue is posted to the Web site.